Catalysis Today 183 (2012) 17–25

Contents lists available at ScienceDirect

Catalysis Today

journal homepage: www.elsevier.com/locate/cattod

Hydroxyapatite-supported cobalt(0) nanoclusters as efficient and cost-effective catalyst for hydrogen generation from the hydrolysis of both sodium borohydride and ammonia-borane

Murat Rakap, Saim Özkar*

Department of Chemistry, Middle East Technical University, 06800 Ankara, Turkey

ARTICLE INFO

Article history:
Received 9 March 2011
Received in revised form 12 April 2011
Accepted 13 April 2011
Available online 10 May 2011

Keywords:
Hydroxyapatite
Cobalt
Nanoclusters
Sodium borohydride
Ammonia-borane
Hydrolysis
Hydrogen

ABSTRACT

Herein, we report the preparation, characterization, and catalytic use of cobalt(0) nanoclusters supported on hydroxyapatite in the hydrolysis of both basic sodium borohydride and ammonia-borane solutions. They were prepared in situ from the reduction of cobalt(II) ions adsorbed on hydroxyapatite with sodium borohydride. Hydroxyapatite-supported cobalt(0) nanoclusters were stable enough to be isolated as solid material and characterized by inductively coupled plasma optical emission spectroscopy (ICP-OES), X-ray diffraction (XRD), attenuated total reflectance infrared (ATR-IR) spectroscopy, X-ray photoelectron spectroscopy (XPS), transmission electron microscopy (TEM), scanning electron microscopy (SEM), and energy dispersive X-ray (EDX) spectroscopy. They are isolable, redispersible, highly active, and cost-effective catalysts for hydrogen generation from the hydrolysis of both sodium borohydride and ammonia-borane even at low concentrations and temperature, providing 25,600 and 7400 turnovers and maximum hydrogen generation rates of 5.0 and 2.2 L H_2 min^{-1} $(g\,Co)^{-1}$ by the hydrolysis of $NaBH_4$ and H_3NBH_3 at 25.0 ± 0.1 °C, respectively. Hydroxyapatite-supported cobalt(0) nanoclusters provide activation energy of 53 ± 2 kJ/mol for the hydrolysis of sodium borohydride and 50 ± 2 kJ/mol for the hydrolysis of ammonia-borane.

© 2011 Elsevier B.V. All rights reserved.

1. Introduction

There has been an increasing demand for the renewable energy sources due to the depletion of fossil fuel resources, environmental pollution, and global warming caused by a steep increase in concentration of carbon dioxide and other greenhouse gases in the atmosphere [1–4]. Hydrogen has been considered as a clean and environmentally benign new energy carrier for heating, transportation, mechanical power and electricity generation [5,6]. However, the storage of hydrogen is still a challenge for the implementation of hydrogen economy [7]. Among the chemical hydrides tested as solid hydrogen storage materials, $NaBH_4$ appears to be a suitable hydrogen source due to a number of advantageous properties such as the high hydrogen storage capacity (10.8 wt.%) which meets the US-DOE criteria for hydrogen storage materials [1], the high stability and non-flammability of its alkaline solutions, the optimal control on hydrogen generation rate by supported catalysts, the acceptable hydrogen generation rate even at low temperature, the availability and easy handling [8–13]. From the recent studies [14–23], ammonia-borane (H_3NBH_3) can also be regarded as a solid hydrogen storage material due to its higher hydrogen content (19.6 wt.%) compared to sodium borohydride and high solubility and stability in water at room temperature [24–32]. Therefore, unlike sodium borohydride solutions, ammonia-borane solutions do not require any additional stabilization using bases. Both sodium borohydride and ammonia-borane liberate hydrogen upon hydrolysis at room temperature in the presence of suitable catalysts according to Eqs. (1) and (2), respectively.

$$NaBH_4(aq) + 2H_2O(l) \xrightarrow{\text{catalyst}} NaBO_2(aq) + 4H_2(g) \quad (1)$$

$$H_3NBH_3(aq) + 2H_2O(l) \xrightarrow{\text{catalyst}} NH_4^+(aq) + BO_2^-(aq) + 3H_2(g) \quad (2)$$

Since the activity of a heterogeneous catalyst is directly proportional to its surface area, the use of metal(0) nanoclusters as catalyst in these hydrolysis reactions is a promising way to increase the catalytic activity [33]. Recently, we have shown that transition metal(0) nanoclusters can be used as highly active heterogeneous catalysts in the hydrolysis of sodium borohydride [34–38] and/or ammonia-borane [39–44]. Herein, we report the preparation, characterization, and employment of cobalt(0) nanoclusters supported on hydroxyapatite as highly active catalyst for hydrogen generation from the hydrolysis of both sodium borohydride

* Corresponding author. Tel.: +90 312 210 3212; fax: +90 312 210 3200.
E-mail address: sozkar@metu.edu.tr (S. Özkar).

0920-5861/$ – see front matter © 2011 Elsevier B.V. All rights reserved.
doi:10.1016/j.cattod.2011.04.022

and ammonia-borane. Hydroxyapatite ($Ca_{10}(PO_4)_6(OH)_2$, HAP) is the main inorganic constituent of bones and can be used as biomaterials, adsorbents, or ion exchangers [45]. We were stimulated to use HAP as matrix in stabilizing metal nanoparticles by the following advantages [46]: (i) HAP has nonporous structure and does not cause significant mass transfer limitation, (ii) it has high ion exchange ability and adsorption capacity, and (iii) its low surface acidity prevents side reactions arising from the support itself. Cobalt(0) nanoclusters supported on hydroxyapatite, hereafter referred to Co(0)-HAP, were in situ prepared from the reduction of cobalt(II) ions adsorbed on the surface of hydroxyapatite (Co^{2+}-HAP) with sodium borohydride. The cobalt(0) nanoclusters supported on hydroxyapatite were isolated as solid material and characterized by inductively coupled plasma optical emission spectroscopy (ICP-OES), X-ray diffraction (XRD), attenuated total reflectance infrared (ATR-IR) spectroscopy, X-ray photoelectron spectroscopy (XPS), transmission electron microscopy (TEM), scanning electron microscopy (SEM), and energy dispersive X-ray (EDX) spectroscopy. The kinetics of the hydrolysis reactions were studied by measuring the volume of hydrogen gas generated, varying catalyst concentration, substrate concentration, and temperature. Our report also includes the results of study on the effect of NaOH concentration on the catalytic activity of Co(0)-HAP nanoclusters in the hydrolysis of sodium borohydride. Co(0)-HAP nanoclusters were found to be highly active and long-lived catalyst providing 25,600 and 7400 turnovers in the hydrolysis of sodium borohydride and ammonia-borane, respectively, at 25.0 ± 0.1 °C. The high catalytic activity, long lifetime, and low cost of Co(0)-HAP nanoclusters make them a promising candidate to be used as catalyst in developing highly efficient portable hydrogen generation systems using sodium borohydride or ammonia-borane as solid hydrogen storage material.

2. Experimental

2.1. Materials

Cobalt(II) nitrate hexahydrate (98%), sodium borohydride (98%), ammonia-borane (>97%), hydroxyapatite, sodium hydroxide, and D_2O were purchased from Aldrich and used as received. Deionized water was distilled by a water purification system (Milli-Q system). All glassware and Teflon-coated magnetic stir bars were cleaned with acetone, followed by copius rinsing with distilled water before drying in an oven at 150 °C.

2.2. In situ preparation of hydroxyapatite-supported cobalt(0) nanoclusters

Hydroxyapatite (1.0 g) was added to a solution of cobalt(II) nitrate hexahydrate (60.5 mg) in 100 mL H_2O in a 250 mL round bottom flask. This slurry was stirred at room temperature for 72 h. During this process, Ca^{2+} ions which act as charge balancing cations in the framework of hydroxyapatite were replaced by Co^{2+} ions. The Co^{2+}-exchanged hydroxyapatite (Co^{2+}-HAP) sample was filtered using Whatman-1 filter paper, washed three times with 20 mL of deionized water, and dried in the oven at 80 °C. Then, Co^{2+}-exchanged hydroxyapatite (Co^{2+}-HAP) sample was reduced during the hydrolysis of sodium borohydride and in situ formation of hydroxyapatite-supported cobalt(0) nanoclusters was obtained. For the hydrolysis of ammonia-borane, the pre-formed hydroxyapatite-supported cobalt(0) nanoclusters were dried under nitrogen atmosphere and used as catalyst for this hydrolysis reaction. The cobalt content of the sample was found to be 0.72 wt.% by ICP-OES.

2.3. Method for testing the catalytic activity of hydroxyapatite-supported cobalt(0) nanoclusters in the hydrolysis of sodium borohydride and ammonia-borane

The catalytic activity of the in situ formed hydroxyapatite-supported cobalt(0) nanoclusters in the hydrolysis of sodium borohydride or ammonia-borane in aqueous solution was determined by measuring the rate of hydrogen generation. In all the experiments, a jacketed reaction flask (75 mL) containing a Teflon-coated stir bar was placed on a magnetic stirrer (Heidolph MR-301) and thermostated to 25.0 ± 0.1 °C by circulating water through its jacket from a constant temperature bath. Then, a graduated glass tube (50 cm in height and 5.0 cm in diameter) filled with water was connected to the reaction flask to measure the volume of the hydrogen gas to be evolved from the reaction. In a typical experiment, 284 mg (7.47 mmol) of $NaBH_4$ or 63.6 mg (2 mmol) of H_3NBH_3 was dissolved in 50 mL and 20 mL of water, respectively. The solutions were transferred with a glass pipet into the reaction flask thermostated at 25.0 ± 0.1 °C. Then, 818.5 mg (327.4 mg for hydrolysis of AB) powder of Co^{2+}-HAP (0.72 wt.% Co) was added into the reaction flask. The experiment was started by closing the flask and the volume of hydrogen gas evolved was measured by recording the displacement of water level at the stirring speed of 900 rpm. In addition to the volumetric measurement of the hydrogen evolution, the conversion of sodium borohydride ($\delta = -42.1$ ppm) [47] and ammonia-borane ($\delta = -23.9$ ppm) [48] to borate ($\delta = 9$–18 ppm) [47,48] was checked by ^{11}B NMR spectroscopy.

2.4. Effect of sodium hydroxide concentration on catalytic activity of hydroxyapatite-supported cobalt(0) nanoclusters in the hydrolysis of sodium borohydride

To examine the effect of sodium hydroxide concentration on the catalytic activity of the hydroxyapatite-supported cobalt(0) nanoclusters in the hydrolysis of sodium borohydride, five different experiments were carried out starting with 50 mL aqueous solution of 150 mM of $NaBH_4$ and different amounts of NaOH (5.0, 7.5, 10.0, 12.5, and 15.0 wt.%) in the presence of hydroxyapatite-supported cobalt(0) nanoclusters (2.0 mM) at 25.0 ± 0.1 °C. All the experiments were performed in the same way as described in Section 2.3.

2.5. Control experiments

2.5.1. The effect of stirring speed on the hydrogen generation rate

In order to check whether the system is under mass transfer limitation, the same experiment for hydrogen generation from the hydrolysis of both sodium borohydride and ammonia-borane was performed as described in Section 2.3 at 25.0 ± 0.1 °C by varying the stirring speed (0, 200, 400, 600, 800, 1000, and 1200 rpm).

2.5.2. Hydroxyapatite-catalyzed hydrolysis of sodium borohydride and ammonia-borane

In order to check the catalytic activity of hydroxyapatite in the hydrolysis of sodium borohydride and ammonia-borane, 284 mg of sodium borohydride or 63.6 mg of ammonia-borane was dissolved in 50 mL (containing 10 wt.% NaOH) and 20 mL of water, respectively, in a jacketed reaction flask thermostated at 25.0 ± 0.1 °C. Then, hydroxyapatite (819 mg) was added to the solution. The volume of generated hydrogen was measured exactly in the same way as described in Section 2.3.

2.6. Kinetic study of the hydrolysis of basic sodium borohydride and ammonia-borane catalyzed by hydroxyapatite-supported cobalt(0) nanoclusters

In order to establish the rate laws for the catalytic hydrolysis of basic sodium borohydride and ammonia-borane using hydroxyapatite-supported cobalt(0) nanoclusters (with 0.72 wt.% cobalt loading), two different sets of experiments were performed in the same way as described in Section 2.3 for each of these substrates. In the first set of experiments, the concentration of the substrate was kept constant (at 150 mM for $NaBH_4$ and 100 mM for H_3NBH_3) and the cobalt concentration was varied in the range of 1.0, 1.5, 2.0, 2.5, and 3.0 mM. In the second set of experiments, cobalt concentration was kept constant at 2.0 mM and substrate concentrations were varied in the range of 150, 300, 450, 600, and 750 mM for $NaBH_4$; and 100, 200, 300, and 400 mM for H_3NBH_3. For the hydrolysis of $NaBH_4$, 10 wt.% of NaOH was used. Finally, the catalytic hydrolysis of basic sodium borohydride and ammonia-borane in the presence of hydroxyapatite-supported cobalt(0) nanoclusters at constant substrate (150 mM for $NaBH_4$ and 100 mM for H_3NBH_3) and cobalt (2.0 mM) concentrations at various temperatures in the range of 15–45 °C for $NaBH_4$ and 25–45 °C for H_3NBH_3 in order to obtain the activation energy (*Ea*).

2.7. Isolability and reusability of hydroxyapatite-supported cobalt(0) nanoclusters in the hydrolysis of sodium borohydride and ammonia-borane

After the first run of the hydrolysis of 150 mM of $NaBH_4$ (284 mg in 50 mL, in the presence of 10 wt.% NaOH) or 100 mM of H_3NBH_3 (63.6 mg in 20 mL), catalyzed by hydroxyapatite-supported cobalt(0) nanoclusters (818.5 mg, or 327.4 mg for AB hydrolysis, Co^{2+}-HAP with a cobalt content 0.72 wt.%, [Co] = 2.0 mM) at 25 °C, the catalyst was isolated by suction filtration, washed with deionized water, and dried under nitrogen atmosphere at room temperature. The isolated and dried samples of hydroxyapatite-supported cobalt(0) nanoclusters were used again in the hydrolysis of 150 mM of basic $NaBH_4$ or 100 mM of H_3NBH_3 and the same procedure was repeated five times. The results were expressed as % initial catalytic activity of hydroxyapatite-supported cobalt(0) nanoclusters in the hydrolysis of basic $NaBH_4$ or H_3NBH_3 solution.

2.8. Determination of the catalytic lifetime of hydroxyapatite-supported cobalt(0) nanoclusters in the hydrolysis of sodium borohydride or ammonia-borane

The catalytic lifetime of the hydroxyapatite-supported cobalt(0) nanoclusters in the hydrolysis of sodium borohydride and ammonia-borane was determined by measuring the total turnover number (TTO). This experiment was started with a 50 mL (or 20 mL for H_3NBH_3) solution containing 2.0 mM hydroxyapatite-supported cobalt(0) nanoclusters and 1 M substrate, $NaBH_4$ or H_3NBH_3 at 25.0 ± 0.1 °C. For the hydrolysis of $NaBH_4$, 10 wt.% NaOH was used. When the complete conversion is achieved, more substrate is added into the solution and the reaction was continued by this way until the catalyst is deactivated in both reactions at 25.0 ± 0.1 °C.

2.9. Characterization of hydroxyapatite-supported cobalt(0) nanoclusters

The cobalt content of the samples was determined by ICP-OES (Leeman-Direct Reading Echelle). For this purpose, the samples were dissolved in a mixture of nitric acid and hydrochloric acid. The cobalt content of the catalyst was found to be 0.72 wt.%. Powder X-ray diffraction (XRD) patterns were recorded with a Rigaku X-ray Diffractometer using Cu Kα radiation (30 kV, 15 mA) at room temperature. Scanning was performed between 5° and 70° 2θ. The measurements were made with 0.01° and 0.05° steps and 1°/min rate. The divergence slit was variable and scattering and receiving slit were 4.2° and 0.3 mm, respectively. Transmission electron microscopy (TEM) analysis was carried out using a JEOL-2010 microscope operating at 200 kV, fitted with a LaB_6 filament and has lattice and theoretical point resolutions of 0.14 nm and 0.23 nm, respectively. Samples were examined at magnification between 100 and 1000 K. One drop of dilute suspension of sample in isopropyl alcohol was deposited on the TEM grids and the solvent was then evaporated. Scanning electron microscopy analysis was carried out using a Quanta 200 FEG environmental scanning electron microscope (ESEM) operating at an accelerating voltage of 30 kV. SEM samples on quartz surfaces were coated with about 4 nm of Pt/Au alloy. ATR-IR spectra were taken on Vartex-70 spectrophotometer using Omnic software. The X-ray photoelectron spectroscopy (XPS) analysis of the catalyst was performed on a Physical Electronics 5800 spectrometer equipped with a hemispherical analyzer and using monochromatic Al Kα lines of Al (1486.6 eV, 10 mA) as an X-ray source. ^{11}B NMR spectra were recorded on a Bruker Avance DPX 400 with an operating frequency of 128.15 MHz for ^{11}B.

3. Results and discussion

3.1. Preparation and characterization of hydroxyapatite-supported cobalt(0) nanoclusters

Hydroxyapatite-supported cobalt(0) nanoclusters were prepared at room temperature following a two step procedure: hydroxyapatite was first added to the aqueous solution of cobalt(II) nitrate and the suspension is stirred for 3 days at room temperature. After filtering, copious washing with water, and drying in the oven at 80 °C, Co^{2+}-exchanged hydroxyapatite (Co^{2+}-HAP) samples were obtained. Then, cobalt(II) ions were reduced to cobalt(0) nanoclusters on the hydroxyapatite surface during the catalytic hydrolysis of sodium borohydride at room temperature. After the complete hydrolysis of sodium borohydride Co(0)-HAP nanoclusters were isolated as solid material by filtration, then dried under inert atmosphere, and characterized by ICP-OES, XRD, ATR-IR, XPS, TEM, SEM, and EDX.

The powder XRD diffraction patterns of the support material hydroxyapatite (HAP) and the Co(0)-HAP nanoclusters are given in

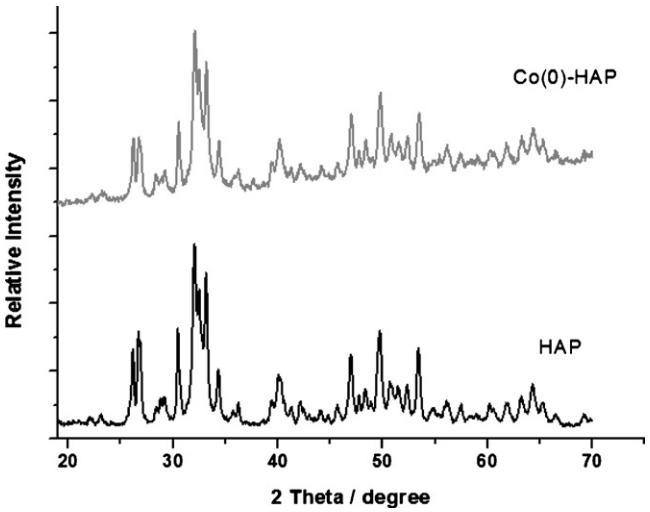

Fig. 1. The powder XRD patterns of the hydroxyapatite as host material and the hydroxyapatite-supported cobalt(0) nanoclusters.

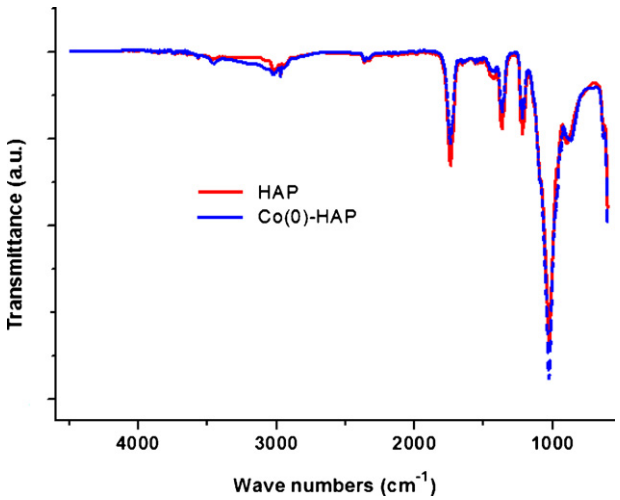

Fig. 2. The ATR-IR spectra of the hydroxyapatite and hydroxyapatite-supported cobalt(0) nanoclusters.

Fig. 1. Two patterns are very similar to each other indicating that the host material remains intact at the end of the procedure without observable alteration in the framework lattice and loss in the crystallinity. The ATR-IR spectra of the support material hydroxyapatite and the Co(0)-HAP nanoclusters are depicted in Fig. 2, which clearly shows that the addition of cobalt to hydroxyapatite framework does not cause any significant change in the IR spectra, confirming the conclusion previously obtained from X-ray diffraction patterns. It is noteworthy that the absence of band at 875 cm^{-1} for the HPO_4^{2-} ion indicates that pyrophosphates are not formed in the samples [46,49]. Additionally, there is no peak attributable to the inclusion of cobalt on the support material in either XRD or IR spectrum because of relatively low cobalt content (0.72 wt.%) of the sample. The morphology, chemical composition, and the particle size of the hydroxyapatite-supported cobalt(0) nanoclusters were studied by SEM, EDX, and TEM as shown in Figs. 3–5, respectively. The EDX analysis shows that cobalt is the only element in the catalyst apart from the host framework elements calcium, oxygen, and phosphorus, indicating the incorporation of cobalt on the support. Additionally, the mapped SEM micrographs show the Ca, O, and P as the host material's framework elements, and Co as the supported element in the catalyst. The TEM image reveals the presence of randomly distributed cobalt(0) nanoclusters with a mean diameter of 3.2 ± 0.8 nm on the HAP surface. Experimental and simulated X-ray photoelectron spectra (XPS) of the Co(0)-HAP nanoclusters sample with a cobalt loading of 0.72 wt.% are given in Fig. 6 which shows two prominent bands at 780 and 796.3 eV, readily attributable to Co(0) $2p_{3/2}$ and Co(0) $2p_{1/2}$, respectively [50]. However, there are two additional bands observed at slightly higher energies, which can be attributed to a higher oxidation states of cobalt, presumably formed by oxidation during the XPS sample preparation, since the cobalt(0) nanoclusters are sensitive to oxygen. These additional weak bands can be attributed to cobalt(II) species, which is likely formed from the oxidation of nanoclusters exposed to air during the XPS sampling [51].

3.2. Effect of sodium hydroxide concentration on catalytic activity of hydroxyapatite-supported cobalt(0) nanoclusters in the hydrolysis of sodium borohydride

Fig. 7 shows the plot of hydrogen generation rate versus NaOH concentration for the hydrolysis of sodium borohydride catalyzed by hydroxyapatite-supported cobalt(0) nanoclusters. The rate of hydrogen generation first increases with the increasing sodium hydroxide concentration, demonstrating an enhancement of reaction by NaOH. It reaches a maximum value at the concentration of 10 wt.% NaOH and subsequently decreases with the further increase in NaOH concentration. This is probably due to the fact that OH^- ion is involved in the hydrolysis of $NaBH_4$ and an appropriate increase in the NaOH concentration can accelerate the hydrolysis reaction and thus hydrogen generation rate. However, excessive NaOH concentration would lead to a decrease in solubility of the hydrolysis by-product, $NaBO_2$. As a result, $NaBO_2$ precipitates from the solution and decreases the hydrogen generation rate, blocking the active sites on the surface of catalyst [52]. Since similar results have been reported [38,52,53] for some cobalt-based catalysts used for hydrogen generation from the hydrolysis of sodium borohydride, it can be concluded that the hydrogen generation rate is not only dependent on the sodium hydroxide concentration of the solution but also on the nature of the catalyst. This observation dictates the use of 10 wt.% NaOH for the kinetic studies of the catalytic hydrolysis of sodium borohydride using hydroxyapatite-supported cobalt(0) nanoclusters as catalyst. A control test was performed to check whether the use of sodium hydroxide causes to leaching of cobalt from the catalyst. ICP analysis of the catalyst sample after catalytic reaction in the presence of 10 wt.% NaOH gave the same cobalt content (0.72 wt.% Co) for the hydroxyapatite-supported cobalt(0) nanoclusters as before the reaction.

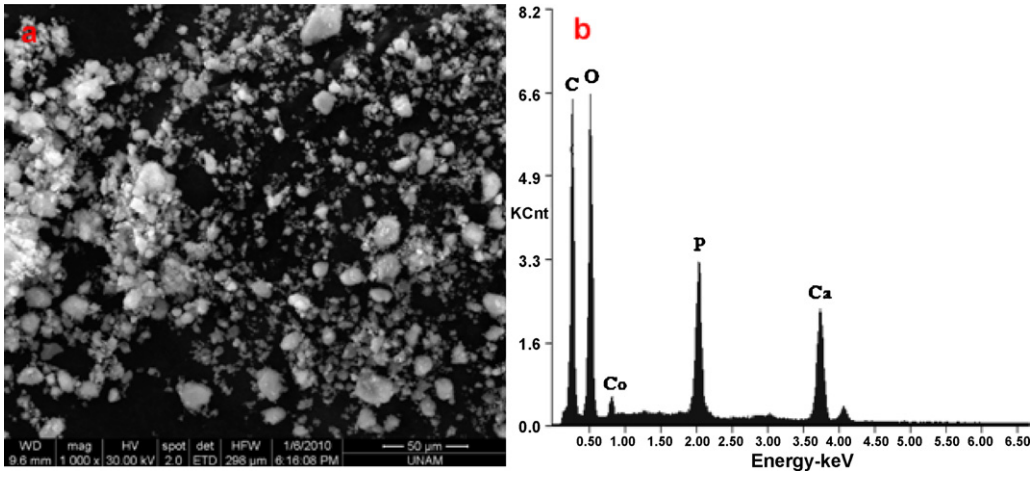

Fig. 3. The typical (a) SEM and (b) EDX images of the hydroxyapatite-supported cobalt(0) nanoclusters with a cobalt loading of 0.72 wt.%.

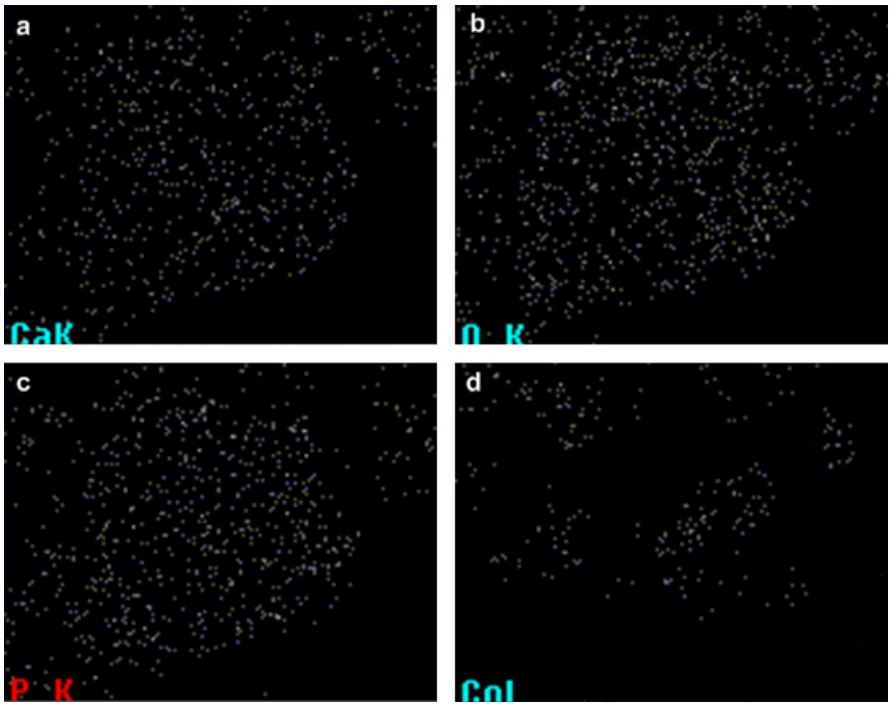

Fig. 4. The mapped SEM micrographs of the elements in the catalyst; (a) Ca, (b) O, (c) P, and (d) Co.

3.3. Control experiments

Before testing the catalytic activity of Co(0)-HAP nanoclusters in the hydrolysis of basic sodium borohydride and ammonia-borane, two control experiments had to be performed: hydrolysis of basic sodium borohydride and ammonia-borane in the presence of hydroxyapatite to check whether hydroxyapatite catalyzes these hydrolysis reactions. No hydrogen gas evolution was observed in the hydrolysis of basic sodium borohydride and ammonia-borane for 24 h in the presence of HAP.

Additionally, the effect of stirring speed on the hydrogen generation rates from the hydrolysis of basic sodium borohydride and ammonia-borane was investigated by carrying out the hydrolysis reactions at different stirring speeds. The results of these control experiments show that the stirring speed has no significant effect on hydrogen generation rate after 600 rpm, for the hydrolysis of both basic sodium borohydride and ammonia-borane. In other words, the system is in a non-mass transfer limitation regime since all the kinetic studies were performed at a stirring speed of 900 rpm.

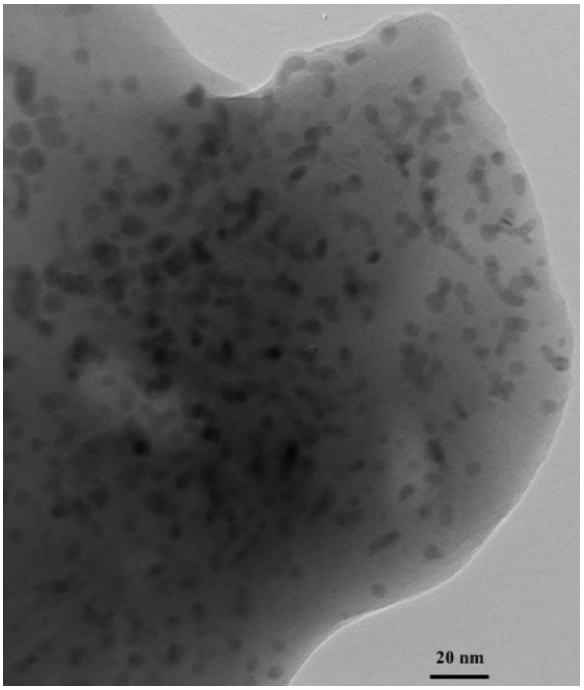

Fig. 5. The TEM image of the hydroxyapatite-supported cobalt(0) nanoclusters with a cobalt loading of 0.72 wt.%.

3.4. Kinetics of hydrolyses catalyzed by hydroxyapatite-supported cobalt(0) nanoclusters

3.4.1. Hydrolysis of sodium borohydride in basic solution

The hydroxyapatite-supported cobalt(0) nanoclusters were found to be highly active catalyst for the hydrolysis of sodium

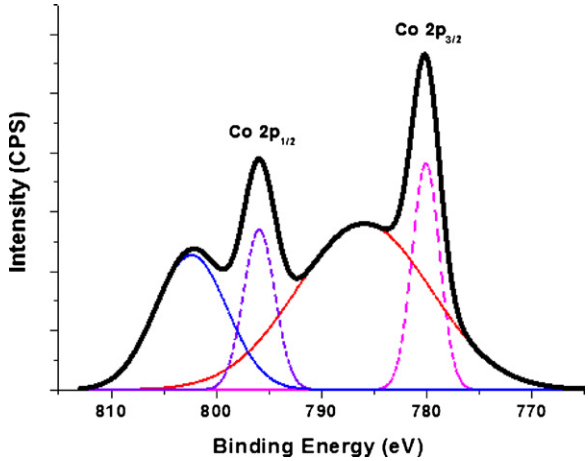

Fig. 6. X-ray photoelectron spectrum of hydroxyapatite-supported cobalt(0) nanoclusters with a cobalt loading of 0.72 wt.%.

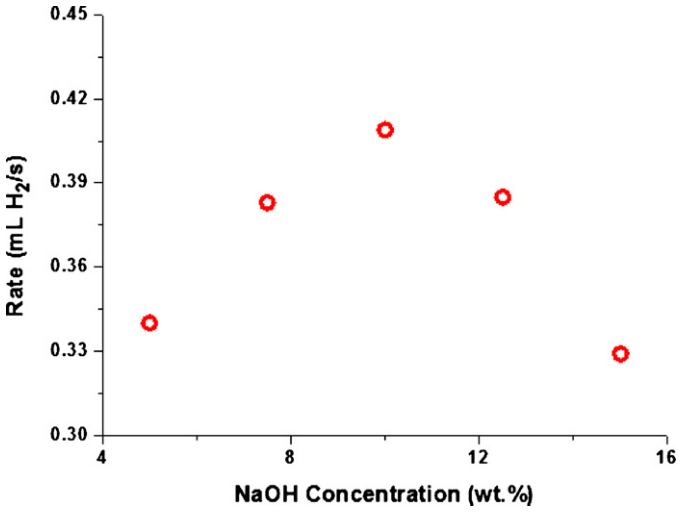

Fig. 7. The plot of hydrogen generation rate versus concentration of NaOH (in wt.%) for the hydrolysis of sodium borohydride (50 mL, 150 mM $NaBH_4$) catalyzed by hydroxyapatite-supported cobalt(0) nanoclusters (2.0 mM Co) at 25.0 ± 0.1 °C.

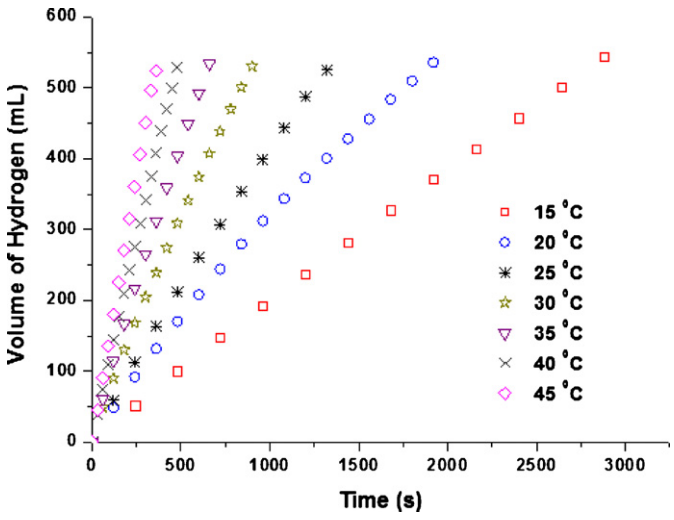

Fig. 9. Plot of the volume of hydrogen (mL) versus time (s) for the hydrolysis of sodium borohydride (50 mL, 150 mM $NaBH_4$) containing 10 wt.% NaOH catalyzed by hydroxyapatite-supported cobalt(0) nanoclusters (2.0 mM Co) at different temperatures in the range 15–45 °C.

borohydride in basic solution. Fig. 8 shows the plot of hydrogen volume versus time during the catalytic hydrolysis of 150 mM $NaBH_4$ solution containing 10 wt.% NaOH in the presence of Co(0)-HAP nanoclusters in different cobalt concentrations at 25.0 ± 0.1 °C. Plotting the hydrogen generation rate, determined from the linear portion of plots in Fig. 8, versus cobalt concentration, both in logarithmic scales (shown in the inset of Fig. 8), gives a straight line with a slope of 1.03 ≈ 1.0 indicating that the hydrolytic dehydrogenation of basic sodium borohydride is first order with respect to the cobalt concentration. The effect of $NaBH_4$ substrate concentration on the hydrolysis rate was also studied by carrying out a series of experiments starting with various initial concentrations of $NaBH_4$ while keeping the catalyst concentration constant at 2.0 mM Co. The hydrogen generation rate was found to be practically independent of the $NaBH_4$ concentration, indicating that the hydrolysis reaction is zero order with respect to the concentration of $NaBH_4$.

Fig. 9 shows the volume of hydrogen generated versus time in the hydrolysis of 150 mM $NaBH_4$ solution containing 10 wt.% NaOH catalyzed by Co(0)-HAP nanoclusters ([Co] = 2.0 mM) at various temperatures. The apparent rate constants (k_{app}) of hydrogen generation from the hydrolysis of basic sodium borohydride were measured from the linear portion of each plot given in Fig. 9 at seven different temperatures in the range of 15–45 °C and used for the calculation of activation energy from the Arrhenius plot (Fig. 10). The apparent Arrhenius activation energy (Ea_{app}) was found to be 53 ± 2 kJ/mol for the hydrolysis of basic sodium borohydride catalyzed by Co(0)-HAP nanoclusters. This value is lower than the activation energies reported in the literature for the same reaction using many different catalysts: 62 kJ/mol for Ni–Co–B [54], 58 kJ/mol for carbon supported Co–B [55], 76 kJ/mol for Ru-promoted sulphated zirconia [56], 70 kJ/mol for Pt/$LiCoO_2$ [57], 68 kJ/mol for Ru/$LiCoO_2$ [55], 56 kJ/mol for Ru/IRA-400 [9], 55 kJ/mol for Co–Mn–B nanocomposite [58], 67 kJ/mol for Ru/C [59], 60 kJ/mol for Co–P [60], but still higher than 34 kJ/mol for intrazeolite cobalt(0) nanoclusters [38], 33 kJ/mol for Co–B/Ni foam [61], 38 kJ/mol for Ni_xB [62], 33 kJ/mol for Co/γ-Al_2O_3 [11], 28 kJ/mol for Pd–C powder [63], 50 kJ/mol for Ru/IR-120 [64], 42 kJ/mol for cobalt powder [65], 45 kJ/mol for Co–B [8], 19 kJ/mol for PtPd-carbon nanotubes [12], 44 kJ/mol for Co/AC [66], and 29 kJ/mol for Co–W–B/Ni [67].

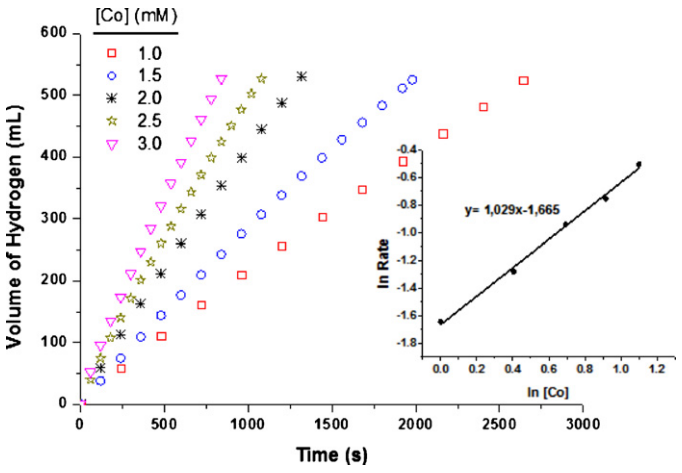

Fig. 8. Plot of the volume of hydrogen (mL) versus time (s) for the hydrolysis of sodium borohydride (50 mL, 150 mM $NaBH_4$) containing 10 wt.% NaOH catalyzed by hydroxyapatite-supported cobalt(0) nanoclusters (2.0 mM Co) with different catalyst concentrations at 25.0 ± 0.1 °C. Inset: plot of the hydrogen generation rate versus the catalyst concentration (both in logarithmic scale) for the same reactions.

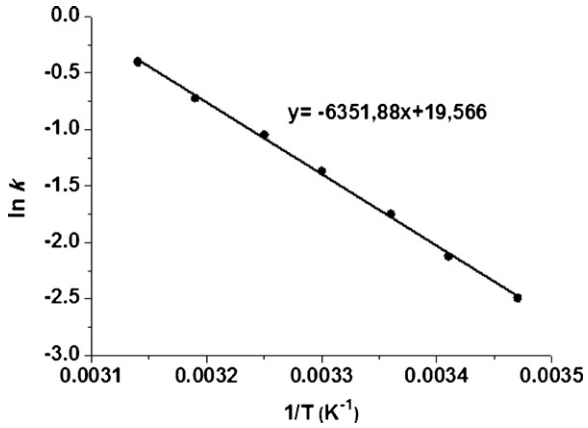

Fig. 10. Arrhenius plot for the hydroxyapatite-supported cobalt(0) nanoclusters catalyzed hydrolysis of $NaBH_4$ containing 10 wt.% NaOH, [$NaBH_4$] = 150 mM, [Co] = 2.0 mM.

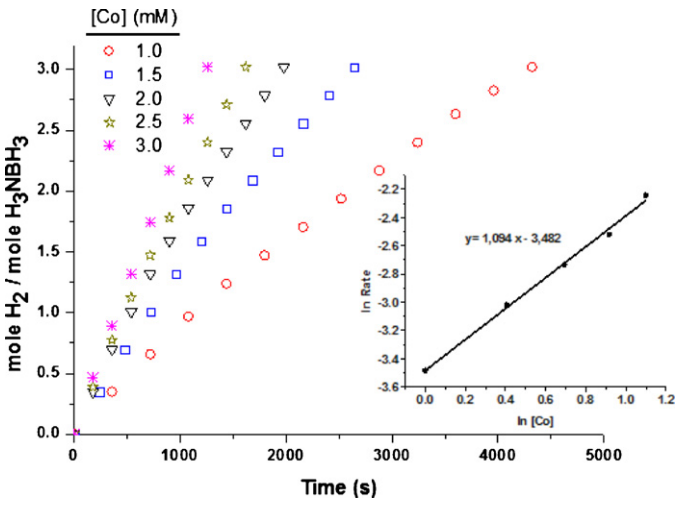

Fig. 11. Plot of mole H_2/mole H_3NBH_3 versus time (s) for the hydrolysis of H_3NBH_3 (20 mL, 100 mM) catalyzed by hydroxyapatite-supported cobalt(0) nanoclusters (2.0 mM Co) with different cobalt concentrations at 25.0 ± 0.1 °C. The inset shows the plot of the hydrogen generation rate versus the catalyst concentration (both in logarithmic scale) for the same reaction.

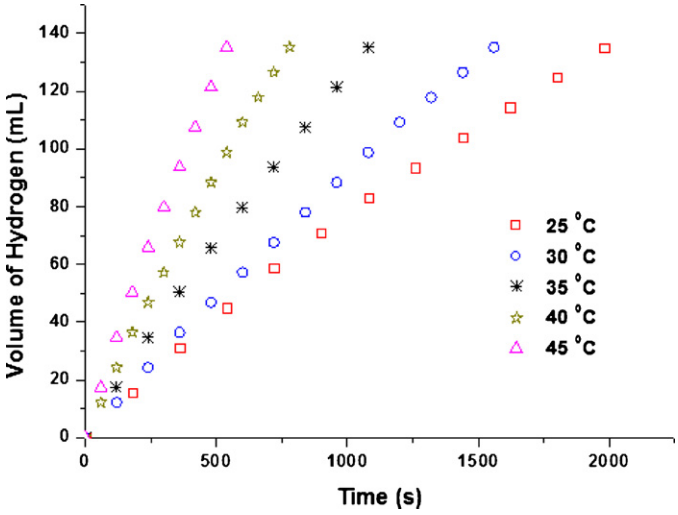

Fig. 12. Plot of the volume of generated hydrogen (mL) versus time (s) for the hydrolysis of H_3NBH_3 (20 mL, 100 mM) catalyzed by hydroxyapatite-supported cobalt(0) nanoclusters (2.0 mM Co) at different temperatures in the range 25–45 °C.

3.4.2. Hydrolysis of ammonia-borane

The hydroxyapatite-supported cobalt(0) nanoclusters were also found to be highly active catalyst for the hydrolysis of ammonia-borane. Fig. 11 shows the plots of the stoichiometric ratio of H_2 to H_3NBH_3 versus time during the catalytic hydrolysis of 100 mM H_3NBH_3 solution in the presence of Co(0)-HAP nanoclusters with a cobalt loading of 0.72 wt.% in different cobalt concentrations at 25.0 ± 0.1 °C. A linear hydrogen generation starts and continues until completion. For example, using Co(0)-HAP nanoclusters in 2.0 mM concentration leads to a complete hydrogen release (3.0 mol H_2/mol H_3NBH_3) within 33 min at 25.0 ± 0.1 °C. Plotting the hydrogen generation rate, determined from the linear portion of each plot in Fig. 11, versus cobalt concentration, both in logarithmic scale (shown in the inset of Fig. 11), gives a straight line with a slope of 1.09 ≈ 1.0 indicating that the hydrolytic dehydrogenation of ammonia-borane is first order with respect to the cobalt concentration. The effect of AB substrate concentration on the hydrolysis rate was also studied by carrying out a series of experiments starting with various initial concentrations of AB while keeping the catalyst concentration constant at 2.0 mM Co. The hydrogen generation rate was found to be practically independent of AB concentration, indicating that the hydrolysis reaction is zero order with respect to the concentration of AB.

The quantity of ammonia liberated during the hydrolysis of ammonia-borane has been found to be negligible when the catalyst concentration is less than 0.06 mol% and the substrate concentration is lower than 6 wt.% [48,65]. Control test using acid/base indicator showed no ammonia evolution in detectable amount in the experiments performed in this study.

Fig. 12 shows the volume of hydrogen generated versus time in the hydrolysis of 100 mM H_3NBH_3 catalyzed by Co(0)-HAP nanoclusters ([Co] = 2.0 mM) at various temperatures. It is worth to note that using Co(0)-HAP nanoclusters in 2.0 mM Co concentration leads to a complete H_2 release (3.0 mol H_2/mol H_3NBH_3) within 33 min corresponding to a hydrogen generation rate of 0.18 mmol H_2 min^{-1}. This provides a total turnover frequency (TOF) value of 4.54 mol H_2 (mol Co)$^{-1}$ min^{-1}, a reasonable value for such a non-noble catalyst compared to the TOF values of other catalysts reported in the literature [68]. The apparent rate constants (k_{app}) of hydrogen generation from the hydrolysis of ammonia-borane were measured from the linear portions of the plots given in Fig. 12 at five different temperatures in the range of 25–45 °C and used for the calculation of activation energy from the Arrhenius plot (Fig. 13). The apparent Arrhenius activation energy (Ea_{app}) was found to be 50 ± 2 kJ/mol for the hydrolysis of ammonia-borane catalyzed by hydroxyapatite-supported cobalt(0) nanoclusters. This value is lower than the activation energies reported in the literature for the same reaction using many different catalysts: 70 kJ/mol for bulk nickel [69], 57 kJ/mol for $Ni_{0.97}Pt_{0.03}$ hollow spheres [69], 62 kJ/mol for Co/γ-Al_2O_3 [24], 63 kJ/mol for PVP-stabilized cobalt(0) nanoclusters [37], 87 kJ/mol for K_2PtCl_6 [15], 76 kJ/mol for Ru/C [27], 56 kJ/mol for zeolite confined palladium(0) nanoclusters [43], 52 kJ/mol for Ni–Ag/C [70], 52 kJ/mol for zeolite confined copper(0) nanoclusters [42], but still higher than 23 kJ/mol for Ru/γ-Al_2O_3 [26], 21 kJ/mol for Rh/γ-Al_2O_3 [26], 21 kJ/mol for Pt/γ-Al_2O_3 [26], 39 kJ/mol for $Pt_{0.65}Ni_{0.35}$ nanoparticles [71], 44 kJ/mol for PSSA-co-MA stabilized Pd(0) nanoclusters [40], 44 kJ/mol for (Co–Mo–B)/Ni foam [72], 22 kJ/mol for Co–P catalyst [73], 34 kJ/mol for Co–B catalyst [74], and 34 kJ/mol for SiO_2-supported monodisperse nickel nanoparticles [75].

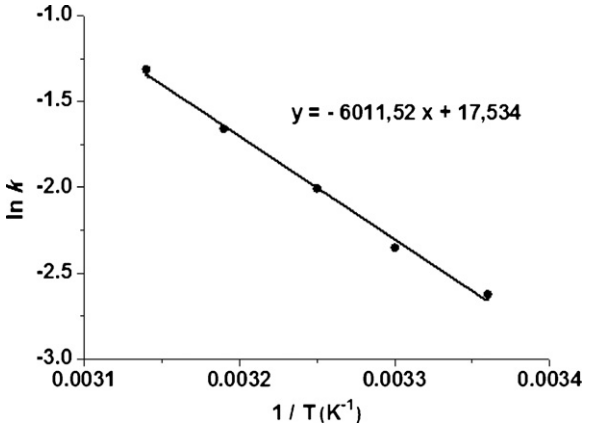

Fig. 13. Arrhenius plot for the hydroxyapatite-supported cobalt(0) nanoclusters catalyzed hydrolysis of H_3NBH_3, [H_3NBH_3] = 100 mM, [Co] = 2.0 mM.

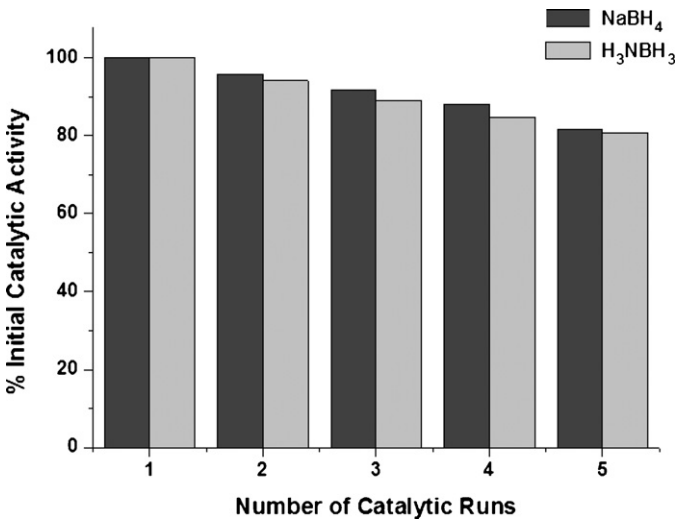

Fig. 14. The % initial catalytic activity retained in the subsequent catalytic runs for hydroxyapatite-supported cobalt(0) nanoclusters catalyzed hydrolysis of basic sodium borohydride and ammonia-borane, separately at 25.0 ± 0.1 °C.

3.5. Isolability and reusability of hydroxyapatite-supported cobalt(0) nanoclusters in the hydrolysis of basic sodium borohydride and ammonia-borane

After the complete hydrolysis of 150 mM basic $NaBH_4$ (or 100 mM H_3NBH_3) solution catalyzed by 2.0 mM Co(0)-HAP nanoclusters at 25 °C, the catalyst was isolated by suction filtration, washed with water, and dried under nitrogen purging at room temperature. The isolated Co(0)-HAP nanoclusters are redispersible in water and yet show activity in the hydrolysis of basic sodium borohydride or ammonia-borane solutions. Fig. 14 shows the changes in catalytic activity of Co(0)-HAP nanoclusters in the hydrolysis of basic sodium borohydride and ammonia-borane in the subsequent catalytic runs at 25.0 ± 0.1 °C. It is noted that Co(0)-HAP nanoclusters retain at least 81% of their initial activity even at the fifth run in the hydrolysis of both basic sodium borohydride and ammonia-borane solutions. These results indicate that Co(0)-HAP nanoclusters are isolable, redispersible, and reusable. In other words, they can be repeatedly used as active catalyst in the hydrolysis of both basic sodium borohydride and ammonia-borane. More importantly, the complete release of hydrogen is obtained in each of the subsequent catalytic runs. Since ICP analysis shows that there is no cobalt leaching into the solution, the slight decrease in catalytic activity in the subsequent runs is probably due to the passivation of nanoclusters surface by increasing amount of metaborate, which might decrease the accessibility of active sites [28,76].

3.6. Catalytic lifetime of hydroxyapatite-supported cobalt(0) nanoclusters in the hydrolysis of sodium borohydride and ammonia-borane

The catalytic lifetime of Co(0)-AP nanoclusters in the hydrolysis reactions of basic sodium borohydride and ammonia-borane solutions was determined by measuring the total turnover numbers in both reactions. The Co(0)-HAP nanoclusters provide 25,600 and 7400 total turnovers in the hydrolysis of basic sodium borohydride and ammonia-borane, respectively, at 25.0 ± 0.1 °C before deactivation.

4. Conclusions

In summary, our study of the preparation and characterization of hydroxyapatite-supported cobalt(0) nanoclusters as catalyst for the hydrolysis of both sodium borohydride and ammonia-borane has led to the following conclusions and insights:

- Hydroxyapatite-supported cobalt(0) nanoclusters can be in situ prepared from the reduction of cobalt(II) ions impregnated on the hydroxyapatite surface during the hydrolysis of sodium borohydride.
- Hydroxyapatite-supported cobalt(0) nanoclusters are highly active catalyst for hydrogen generation from the hydrolysis of basic sodium borohydride and ammonia-borane.
- They are long-lived catalyst providing 25,600 and 7400 turnovers in the hydrolysis of basic sodium borohydride and ammonia-borane, respectively.
- Activation energies for the catalytic hydrolysis of basic sodium borohydride and ammonia-borane in the presence of hydroxyapatite-supported cobalt(0) nanoclusters were calculated as 53 ± 2 and 50 ± 2 kJ/mol, respectively.
- Hydroxyapatite-supported cobalt(0) nanoclusters can be regarded as a promising catalyst with its high activity, lifetime, and low-cost for practical applications to supply hydrogen from the hydrolysis of sodium borohydride or ammonia-borane for proton exchange membrane fuel cells.

Acknowledgements

Partial support of this work by Turkish Academy of Sciences is gratefully acknowledged. M.R. thanks to TUBITAK (Research Fellowship-2211) and METU-DPT-OYP program on behalf of Yuzuncu Yil University. We acknowledge the expert assistance of Dr. Yi-Feng Su and Ana Marcia Erb of Florida State University at the National High Magnetic Field Laboratory (NHMFL) with the TEM and EDX measurements, respectively.

References

[1] Basic Research Needs For the Hydrogen Economy, Report of the Basic Energy Sciences Workshop on Hydrogen Production, Storage and Use, May 13–15, Office of Science, U.S. Department of Energy, 2003, www.sc.doe.gov/bes/hydrogen.pdf.
[2] Annual Energy Outlook 2005 with Projections to 2025, Energy Information Administration, February 2005, www.eia.doe.gov/oiaf/aeo/pdf/0383(2005).pdf.
[3] J. Turner, G. Sverdrup, K. Mann, P.G. Maness, B. Kroposki, M. Ghirardi, R.J. Evans, D. Blake, Int. J. Energy Res. 32 (2008) 379–407.
[4] C.H. Liu, B.H. Chen, C.L. Hsueh, J.R. Ku, M.S. Jeng, F. Tsau, Int. J. Hydrogen Energy 34 (2009) 2153–2163.
[5] D.A.J. Rand, R.M. Dell, J. Power Sources 144 (2005) 568–578.
[6] J. Zhang, T.S. Fisher, J.P. Gore, D. Hazra, P.V. Ramachandran, Int. J. Hydrogen Energy 31 (2006) 2292–2298.
[7] Q. Zhang, G.M. Smith, Y. Wu, Int. J. Hydrogen Energy 32 (2007) 4731–4735.
[8] J. Lee, K.Y. Kong, C.R. Jung, E. Cho, S.P. Yoon, J. Han, T.G. Lee, S.W. Nam, Catal. Today 120 (2007) 305–310.
[9] S.C. Amendola, J.M. Janjua, N.C. Spencer, M.T. Kelly, P.J. Petillo, S.L. Sharp-Goldman, M. Binder, Int. J. Hydrogen Energy 25 (2000) 969–975.
[10] Y. Kojima, K.I. Suzuki, K. Fukumoto, M. Sasaki, T. Yamamoto, Y. Kawai, H. Hayashi, Int. J. Hydrogen Energy 27 (2002) 1029–1034.
[11] W. Ye, H. Zhang, D. Xu, L. Ma, B. Yi, J. Power Sources 164 (2007) 544–548.
[12] R.P. Alonso, A. Sicurelli, E. Callone, G. Carturan, R. Raj, J. Power Sources 165 (2007) 315–323.
[13] N. Patel, G. Guella, A. Kale, A. Miotello, B. Patton, C. Zanchetta, R. Fernandes, J. Phys. Chem. C 112 (2008) 6968–6976.
[14] F.H. Stephens, V. Pons, R.T. Baker, Dalton Trans. (2007) 2613–2626.
[15] N. Mohajeri, A. T-Raissi, O. Adebiyi, J. Power Sources 167 (2007) 482–485.
[16] T. Umegaki, J.M. Yan, X.B. Zhang, H. Shioyama, N. Kuriyama, Q. Xu, Int. J. Hydrogen Energy 34 (2008) 2303–2311.
[17] P.V. Ramachandran, P.D. Gagare, Inorg. Chem. 46 (2007) 7810–7817.
[18] T. Umegaki, J.M. Yan, X.B. Zhang, H. Shioyama, N. Kuriyama, Q. Xu, J. Power Sources 195 (2010) 8209–8214.
[19] A. Staubitz, A.P.M. Robertson, I. Manners, Chem. Rev. 110 (2010) 4079–4124.
[20] P. Wang, X.D. Kang, Dalton Trans. (2008) 5400–5413.
[21] A. Karkamkar, C. Aardahl, T. Autrey, Mater. Matters 2 (2007) 6–10.
[22] B. Peng, J. Chen, Energy Environ. Sci. 1 (2008) 479–483.
[23] N.C. Smythe, J.C. Gordon, Eur. J. Inorg. Chem. (2010) 509–521.
[24] Q. Xu, M. Chandra, J. Power Sources 163 (2006) 364–370.
[25] Q. Xu, M. Chandra, J. Alloys Compd. 446–447 (2007) 729–732.

[26] M. Chandra, Q. Xu, J. Power Sources 168 (2007) 135–142.
[27] S. Basu, A. Brockman, P. Gagare, Y. Zheng, P.V. Ramachandran, W.N. Delgass, J. Power Sources 188 (2009) 238–243.
[28] T.J. Clark, G.R. Whittell, I. Manners, Inorg. Chem. 46 (2007) 7522–7527.
[29] S.B. Kalidindi, U. Sanyal, B.R. Jagirdar, Phys. Chem. Chem. Phys. 10 (2008) 5870–5874.
[30] T. Umegaki, J.M. Yan, X.B. Zhang, H. Shioyama, N. Kuriyama, Q. Xu, J. Power Sources 191 (2009) 209–216.
[31] T. Umegaki, J.M. Yan, X.B. Zhang, H. Shioyama, N. Kuriyama, Q. Xu, Int. J. Hydrogen Energy 34 (2009) 3816–3822.
[32] J.M. Yan, X.B. Zhang, S. Han, H. Shioyama, Q. Xu, Angew. Chem. Int. Ed. 47 (2008) 2287–2289.
[33] S. Özkar, Appl. Surf. Sci. 256 (2009) 1272–1277.
[34] Ö. Metin, S. Özkar, Int. J. Hydrogen Energy 32 (2007) 1707–1715.
[35] M. Zahmakıran, S. Özkar, J. Mol. Catal. A: Chem. 258 (2006) 95–103.
[36] M. Zahmakiran, S. Özkar, Langmuir 25 (2009) 2667–2678.
[37] Ö. Metin, S. Özkar, Energy Fuels 23 (2009) 3517–3526.
[38] M. Rakap, S. Özkar, Appl. Catal. B 91 (2009) 21–29.
[39] M. Zahmakıran, S. Özkar, Appl. Catal. B 89 (2009) 104–110.
[40] Ö. Metin, Ş. Şahin, S. Özkar, Int. J. Hydrogen Energy 34 (2009) 6304–6313.
[41] F. Durap, M. Zahmakıran, S. Özkar, Int. J. Hydrogen Energy 34 (2009) 7223–7230.
[42] M. Zahmakıran, F. Durap, S. Özkar, Int. J. Hydrogen Energy 35 (2010) 187–197.
[43] M. Rakap, S. Özkar, Int. J. Hydrogen Energy 35 (2010) 1305–1312.
[44] M. Rakap, S. Özkar, Int. J. Hydrogen Energy 35 (2010) 3341–3346.
[45] K. Mori, T. Hara, T. Mizugaki, K. Ebitani, K. Kaneda, J. Am. Chem. Soc. 126 (2004) 10657–10666.
[46] B.C. Gates, Chem. Rev. 95 (1995) 511–522.
[47] G. Guella, C. Zanchetta, B. Patton, A. Miotello, J. Phys. Chem. B 110 (2006) 17024–17033.
[48] M. Chandra, Q. Xu, J. Power Sources 156 (2006) 190–194.
[49] K. Elkabouss, M. Kacimi, M. Ziyad, S. Ammar, F. Bozon-Verduraz, J. Catal. 226 (2004) 16–24.
[50] A.B. Mandale, S. Badrinarayanan, S.K. Date, A.P.B. Sinha, J. Electron Spectrosc. Relat. Phenom. 33 (1984) 61–72.
[51] N.S. McIntyre, M.G. Cook, Anal. Chem. 47 (1975) 2208–2213.
[52] X.L. Ding, X. Yuan, C. Jia, Z.F. Ma, Int. J. Hydrogen Energy 35 (2010) 11077–11084.
[53] M. Rakap, E.E. Kalu, S. Özkar, Int. J. Hydrogen Energy 36, (2011), doi:10.1016/j.jallcom.2011.04.023.
[54] J.C. Ingersoll, N. Mani, J.C. Thenmozhiyal, A. Muthaiah, J. Power Sources 173 (2007) 450–457.
[55] J. Zhao, H. Ma, J. Chen, Int. J. Hydrogen Energy 32 (2007) 4711–4716.
[56] U.B. Demirci, F. Garin, J. Mol. Catal. A: Chem. 279 (2008) 57–62.
[57] Z. Liu, B. Guo, S.H. Chan, E.H. Tang, L. Hong, J. Power Sources 176 (2008) 306–311.
[58] M. Mitov, R. Rashkov, N. Atanassov, A. Zielonka, J. Mater. Sci. 42 (2007) 3367–3372.
[59] Z.S. Zhang, W.N. Delgass, T.S. Fisher, J.P. Gore, J. Power Sources 164 (2007) 772–781.
[60] K.S. Eom, K.W. Cho, H.S. Kwon, J. Power Sources 180 (2008) 484–490.
[61] H.B. Dai, Y. Liang, P. Wang, H.M. Chang, J. Power Sources 177 (2008) 17–23.
[62] D. Hua, Y. Hanxi, A. Xinping, C. Chuansin, Int. J. Hydrogen Energy 28 (2003) 1095–1100.
[63] N. Patel, B. Patton, C. Zanchetta, R. Fernandes, G. Guella, A. Kale, A. Miotello, Int. J. Hydrogen Energy 33 (2008) 287–292.
[64] C.L. Hsueh, C.Y. Chen, J.R. Ku, S.F. Tsai, Y.Y. Hsu, F. Tsau, M.S. Jeng, J. Power Sources 177 (2008) 485–492.
[65] B.H. Liu, Z.P. Li, S. Suda, J. Alloys Compd. 415 (2006) 288–293.
[66] D. Xu, P. Dai, X. Liu, C. Cao, Q. Guo, J. Power Sources 182 (2008) 616–620.
[67] H.B. Dai, Y. Liang, P. Wang, X.D. Yao, T. Rufford, M. Lu, H.M. Cheng, Int. J. Hydrogen Energy 33 (2008) 4405–4412.
[68] Ö. Metin, V. Mazumder, S. Özkar, S. Sun, J. Am. Chem. Soc. 132 (2010) 1468–1469.
[69] S.B. Kalidindi, M. Indirani, B.R. Jagirdar, Inorg. Chem. 47 (2008) 7424–7429.
[70] C.F. Yao, L. Zhuang, Y.L. Cao, X.P. Hi, H.X. Yang, Int. J. Hydrogen Energy 33 (2008) 2462–2467.
[71] X. Yang, F. Cheng, J. Liang, Z. Tao, J. Chen, Int. J. Hydrogen Energy 34 (2009) 8785–8791.
[72] H.B. Dai, L.L. Gao, Y. Liang, X.D. Kang, P. Wang, J. Power Sources 195 (2010) 307–312.
[73] K.S. Eom, K.W. Cho, H.S. Kwon, Int. J. Hydrogen Energy 35 (2010) 181–186.
[74] N. Patel, R. Fernandes, G. Guella, A. Miotello, Appl. Catal. B 95 (2010) 137–143.
[75] Ö. Metin, S. Özkar, S. Sun, Nano Res. 3 (2010) 676–684.
[76] C.A. Jaska, T.J. Clark, S.B. Clendenning, D. Groeza, A. Turak, Z.H. Lu, I. Manners, J. Am. Chem. Soc. 127 (2005) 5116–5124.